Synthetically Diversified Protein Nanopores: Resolving Click Reaction Mechanisms

Synthetically Diversified Protein Nanopores: Resolving Click Reaction Mechanisms

*Marius M. Haugland, Stefan Borsley, Dominic F. Cairns-Gibson, Alex Elmi and Scott L. Cockroft**

EaStCHEM School of Chemistry, University of Edinburgh, Joseph Black Building, David Brewster Road, Edinburgh EH9 3FJ, United Kingdom.

KEYWORDS: nanopores; nanotechnology; single-molecule; bioconjugation; protein modification; CuAAC; reaction mechanisms;

ABSTRACT: Nanopores are emerging as a powerful tool for the investigation of nanoscale processes at the single-molecule level. Here we demonstrate the methionine-selective synthetic diversification of α-hemolysin (α-HL) protein nanopores, and their exploitation as a platform for investigating reaction mechanisms. A wide range of functionalities, including azides, alkynes, nucleotides and single-stranded DNA, were incorporated into individual pores in a divergent fashion. The ion currents flowing through the modified pores was used to observe the trajectory of a range of azide-alkyne click reactions, and revealed several short-lived intermediates in Cu(I)-catalyzed azide-alkyne [3+2] cycloadditions (CuAAC) at the single-molecule level. Analysis of ion current fluctuations enabled the populations of species involved in rapidly exchanging equilibria to be determined, facilitating the resolution of several transient intermediates in the CuAAC reaction mechanism. The versatile pore-modification chemistry offers a useful approach for enabling future physical organic investigations of reaction mechanisms at the single-molecule level.

Analytical techniques based on transmembrane protein nanopores have become well-established methods for investigating chemical and physical phenomena on the single-molecule level.[1-4] Although less physically robust than solid-state nanopores,[5,6] biological nanopores offer the advantage of having atomically precise structures, thereby providing superior precision and reproducibility in their applications.[2,3,7] Monitoring the current flow through a nanopore under an applied transmembrane potential (voltage) enables the real-time, *in situ* characterization of the interaction between the pore and other molecular entities: any changes in the recorded current can provide information about the molecular structure of an analyte,[8-11] the kinetics and dynamics of non-covalent binding,[8,12-15] or chemical reactivity.[16-23] Biological nanopores have even served as the scaffold for constructing molecular machines.[24-26]

Compared to solid-state nanopores,[6,27-30] the possibilities for tuning the properties of biological protein pores *via* chemical modification are more limited. For example, the dimensions, charge and chemical reactivity of the widely used heptameric α-hemolysin nanopore (α-HL) can be modified by altering the constituent monomer units through site-directed mutagenesis.[9,20,21,31,32] A single modification, typically a cysteine, is then introduced through the stochastic self-assembly of one engineered protein monomer with six wild-type monomers. More recently, non-natural amino acids have been introduced into α-HL nanopores through native chemical ligation of synthetic peptide fragments.[18,19] The introduction of reactive handles through either method has enabled further site-specific decoration of nanopores, and even permitted the observation of reaction intermediates in chemistries popular for bioorthogonal functionalization.[18,20]

Here we have exploited the specific reactivity and low abundance of methionine residues to synthetically diversify individual membrane-embedded wild-type α-HL nanopores with a range of synthetic functional groups (Figure 1). *In situ* functionalization of the nanopore with alkyne and azide linkers (Figure 2) enabled the further diversification of the pores *via* bioorthogonal click reactions (Figure 3). Finally, the utility of this pore-modification approach to enable physical organic mechanistic investigations at the single-molecule level was demonstrated by application to CuAAC reactions (Figure 4). The high spatio-temporal resolution of the method enabled the assignment of several transient and dynamically exchanging reaction intermediates along the pathways of CuAAC reactions (Figures 5–8).

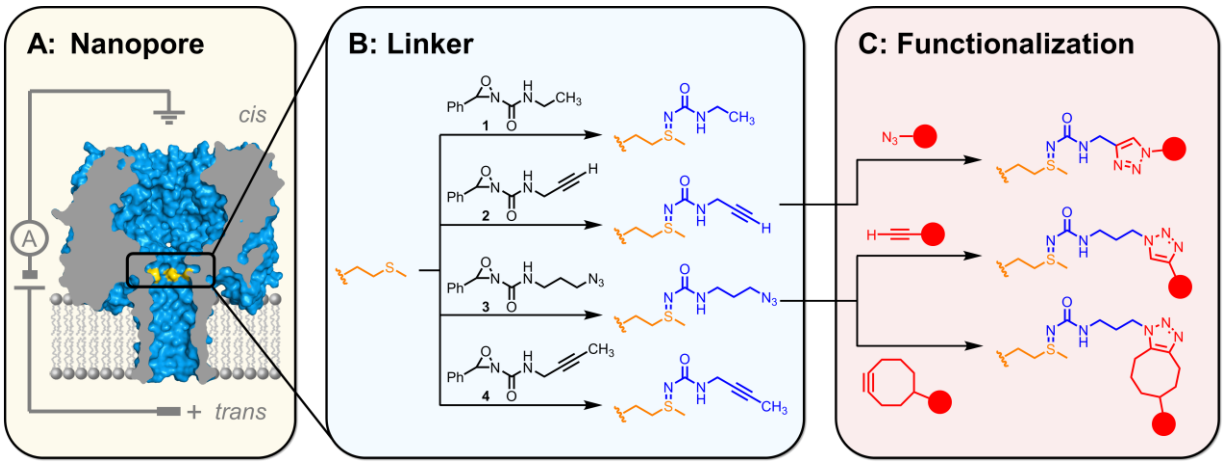

Figure 1. Synthetic diversification of protein nanopores. (A) Experimental setup in which an ion current arises from the flow of ions through a transmembrane α-HL nanopore under an applied voltage. (B) A single methionine residue (yellow) could be modified using oxaziridine reagents (**1**–**4**). (C) The installed linkers were further functionalized in a divergent fashion using popular bioorthogonal click reactions.

RESULTS AND DISCUSSION

In Situ Chemical Functionalization of Methionine Residues

The α-hemolysin (α-HL) protein nanopore, which self-assembles spontaneously into heptameric membrane-spanning channels, is one of the most widely exploited biological nanopores (Figure 1A).[33] The popularity of this nanopore is likely due to its robustness and well-established structure. Although modification of α-HL *via* mutagenesis is possible,[9,20,21,31,32] the commercial availability of α-HL means that it is often used in its wild-type form.[4,8,10-15,22,23,34] Furthermore, cysteine mutants may sometimes present purification or misfolding issues arising from disulfide formation. Recently, fully assembled wild-type α-HL nanopores have been modified *in situ* through direct chemical functionalization of lysine residues.[34] While this approach provided rapid access to nanopores modified within the channel, such residues are both abundant within protein structures and often solvent-exposed, and thus, the modification of other lysine residues could not be fully controlled. Therefore, we sought an alternative, more site-selective method for synthetic modification.

Methionine is one of the least abundant of the 20 canonical amino acids, while its hydrophobic nature means that it is rarely exposed on the surface of proteins.[35] Moreover, only seven methionine residues are exposed within the transmembrane channel of α-HL (one on each subunit, yellow, Figures 1A and S1). We therefore reasoned that the recently developed redox-activated chemical tagging (ReACT) protocol[35] might be utilized for the chemoselective functionalization of α-HL (Figure 1B).

We prepared oxaziridine reagents **1**–**4** (Figure 1B) based on the published procedures (see Supporting Information).[35] Each of these oxaziridine reagents were then introduced to either side of a single membrane-embedded α-HL nanopore (Figures S2–S4) under an applied voltage of +100 mV (Figure 2A). In the presence of 1.7 mM of ethyl derivative **1**, six stepwise decreases in the ion current flowing through the pore were observed over a few minutes (Figure 2B and S8). These steps were attributed to steric blockage of ion current arising from the successive modification of six out of the seven methionine residues within the α-HL channel (steps in Figures 2B, S5, and S6).[36] Similarly, treatment of a single nanopore with the propargyl reagent **2** (Figures 1B, 2C and S9–S11) resulted in complete functionalization at all seven methionine residues. The ability to monitor the modification state of the nanopore in real-time enabled the reaction to be quenched after the incorporation of only a single linker molecule by the addition of 20 eq. of methionine (Figures 2D, S8, S12 and S13). Nanopores were also easily modified using azide reagent **3** and butynyl reagent **4** (Figures 1B, 2E and S14–S17). Modifications were found to occur irrespective of whether the oxaziridine reagent was added to the *cis* or the *trans* side of the nanopore (Figure S13). Thus, we demonstrated the modification of individual nanopores in a site-selective fashion with chemical handles that would enable further synthetic diversification.

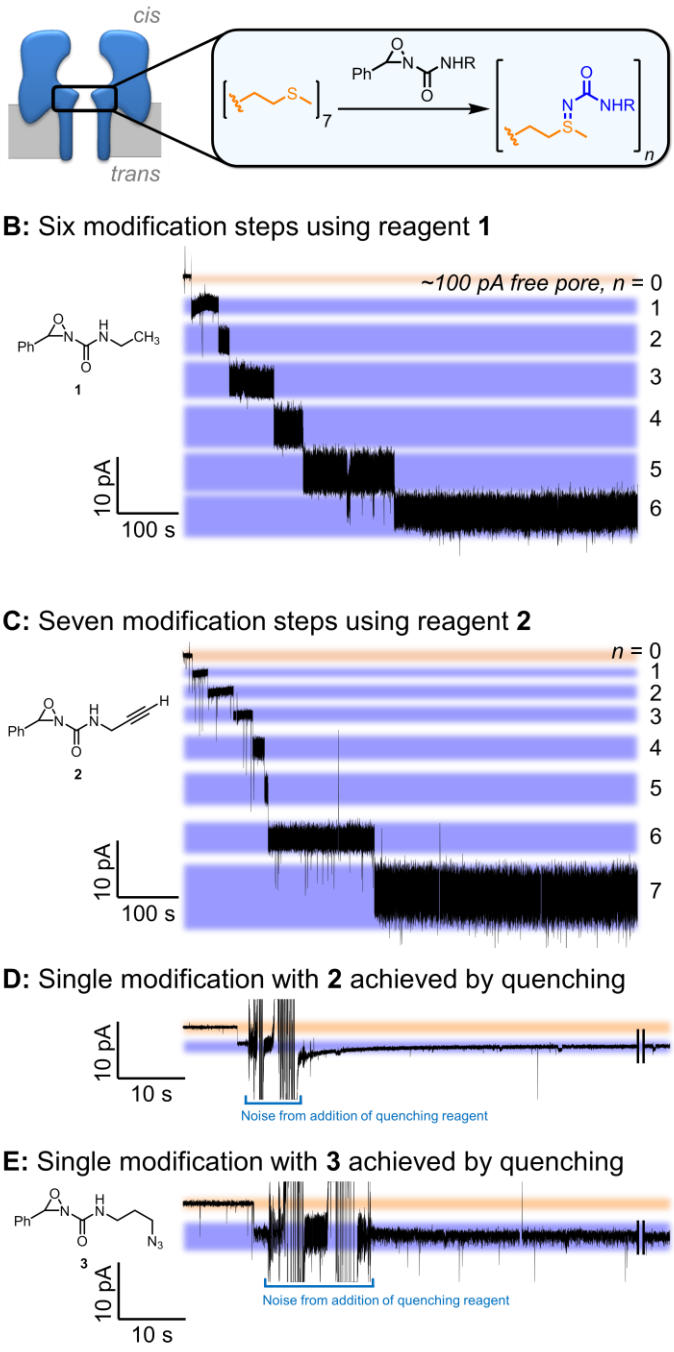

Figure 2. (A) Oxaziridine modification of methionine residues in an α-HL nanopore. (B) Pore modification reaction with **1** (1.7 mM) resulted in six stepwise blockages in the flow of ions though the nanopore indicating six sequential modification reactions (n = 0 to 6). (C)

Modification with **2** (1.7 mM) resulted in full functionalization of all seven methionine residues. (D) Introduction of a single alkyne modification through reaction with **2** (0.17 mM) and quenching by addition of methionine (3.4 mM, 20 equiv.). (E) Introduction of a single azide modification with **3** (0.17 mM) and methionine quenching. All traces were recorded at 298 K, +100 mV in 1 M KCl, 30 mM potassium phosphate buffer (pH 8.0). Small current drops following quenching were due to temporary localized dilution of the electrolyte solution. Free pore currents are indicated in orange. See the Supporting Information for complete experimental traces.

Click Diversification of Nanopores

Having established the ability to control the modification of the methionine residues within the nanopore, we next sought to explore divergent elaboration of the installed linker functionalities. Given the successful installation of azide and propargyl linkers described above, click cycloaddition reactions provide an obvious choice of chemistry to enable further synthetic diversification.[37-39]

Strain-promoted azide-alkyne cycloaddition (SPAAC) was performed on individual nanopores modified with a single azide linker, as indicated by the irreversible drop in the ion current upon addition of cyclooctyne **5** (Figure 3A, top and S18–S20). A larger, but intrinsically more reactive dibenzocyclooctyne was found not to react within the nanopore on a reasonable timescale.[20] Similarly, ion current traces also indicated that in the presence of $CuSO_4$ and sodium ascorbate, a Cu(I)-catalyzed azide-alkyne [3+2] cycloaddition (CuAAC) was successful with alkyne **6** (Figure 3A, bottom and S21–S23).

Encouraged by these results, we moved on to examine CuAAC reactions within nanopores modified with an alkyne linker. Alkyne-bearing nanopores were allowed to react with a range of

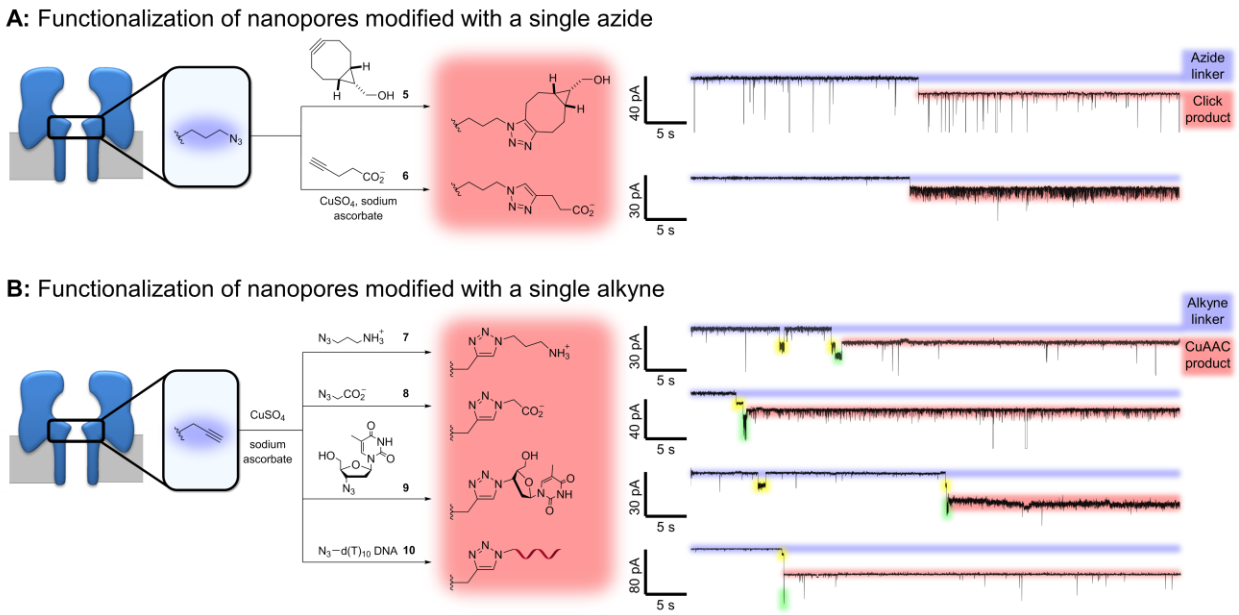

Figure 3. (A) Strain-promoted azide-alkyne cycloaddition (SPAAC) and Cu(I)-catalyzed azide-alkyne [3+2] cycloaddition (CuAAC) reactions on an azide-bearing nanopore. (B) CuAAC reactions on an alkyne-bearing nanopore. All traces were recorded at 298 K, +100 mV in 1 M KCl, 30 mM potassium phosphate buffer (pH 8.0). Copper binding events are highlighted in yellow, and other transient intermediates in green. See the Supporting Information for repeat experiments, including complete traces and detailed experimental conditions.

water-soluble azides (Figure 3B and S24–S40) in the presence of $CuSO_4$ and sodium ascorbate. Gratifyingly, facile CuAAC reactions were observed between the alkyne-bearing nanopore and azides bearing either cationic (**7**) or anionic (**8**) functional groups, as indicated by the ion current changes. Azidonucleotide **9** also took part in a CuAAC reaction, leading to the covalent attachment of a nucleobase near the constriction site; this modification is of particular interest as it could be envisaged as an additional reading head for enhanced-resolution single-molecule DNA sequencing.[40-42] The nanopore could even be functionalized with a $d(T)_{10}$ oligonucleotide carrying an azide at the 3′-terminus (**10**; see SI section 3.2 for detailed structure), giving rise to a

hybrid protein-DNA conjugate.

While the irreversible step-changes in the ion current (and I/V traces, see Supporting Information) are a clear indicator of synthetic diversification of the nanopore, our attention was also drawn to the finer details of the ion current traces. For example, in the CuAAC reactions, reversible blockages were observed that might be attributed to Cu(I)-alkyne complexation (yellow, Figure 3B). In addition, such states were always seen to precede the subsequent irreversible formation of the triazole product *via* a second, short-lived intermediate (yellow to green to red, Figure 3B). These observations provided a tantalizing indication that our modified nanopores might provide the opportunity for gaining mechanistic insights into CuAAC reactions at the single-molecule level.

Single-molecule Investigation of the CuAAC Reaction using Alkyne-modified Nanopores

The mechanism of the CuAAC reaction has been a subject of debate in the literature, with a central issue being the number of copper ions involved (Figure 4A).[43-52] It is generally accepted that a reversible reaction between a terminal alkyne (**12**, Figure 4A) and a copper(I) salt leads to formation of a Cu-alkyne π-complex (**12′**, blue), which is subsequently converted into a copper acetylide (**13**, yellow). From here, the reaction has been proposed to proceed through a mono-Cu pathway (left-hand cycle) by reaction with azide (**14**) to form a copper triazolide (**15**, green) before liberating the product triazole (**16**, red). Alternatively, reaction *via* a two-copper mechanism has also been proposed (right-hand cycle), in which the terminal mono-copper

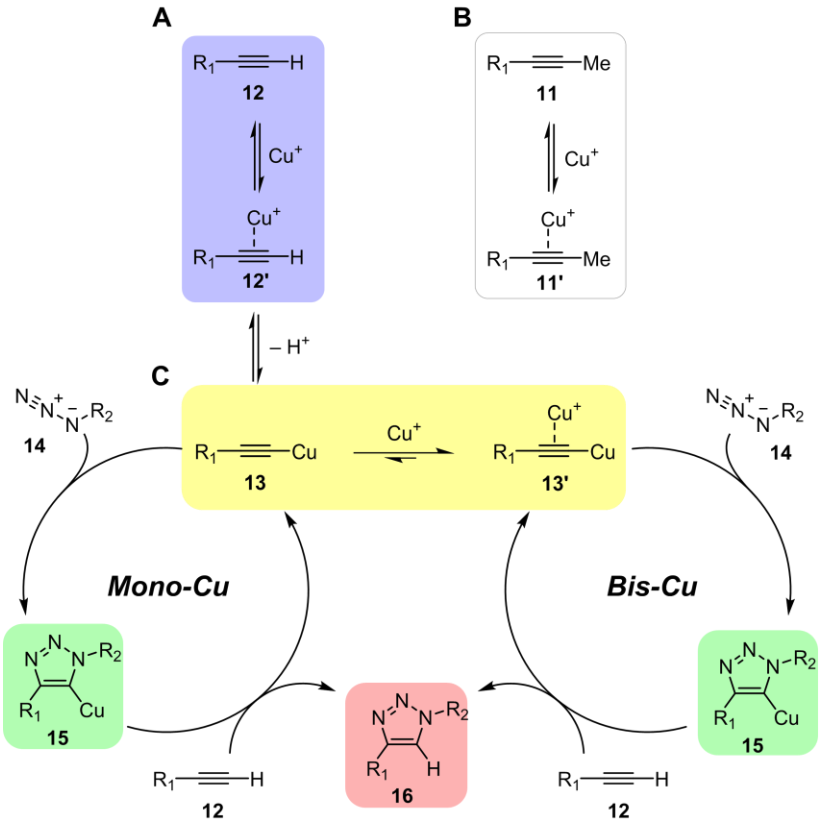

Figure 4. (A) Proposed mechanistic cycles for the CuAAC reaction, *via* either a mono-Cu or bis-Cu pathway.[43] (B) Cu(I) π-complexation with an internal alkyne.

species (**13**, yellow left) binds a second copper ion to form a productive bis-Cu acetylide complex (**13′**, yellow right). For instance, an elegant recent study isolated terminal mono- and bis-Cu complexes and putative intermediates that were stabilized by *N*-heterocyclic carbene (NHC) ligands, and suggested that both mono- and bis-Cu catalytic cycles were in operation, with the latter being kinetically favored.[43] While previous studies have supported a bis-Cu mechanism, such mechanistic investigations have usually required the use of ligands to stabilize

key intermediates, and therefore may not be representative of typical CuAAC synthetic protocols. Thus, the ability to monitor such reactions on the single-molecule level provides the opportunity to resolve short-lived intermediates that would be otherwise difficult to detect *via* ensemble analyses.

Indeed, Bayley and co-workers have previously observed CuAAC reactions on the single-molecule level using semi-synthetic nanopores. These nanopores were assembled from semi-synthetic protein monomers, which were themselves assembled from an alkyne-functionalized peptide and two flanking recombinant polypeptides using native chemical ligation.[18] The authors found that the addition of Cu(I) caused no significant change in the ion current, and thus proposed that if a copper acetylide (**13**) is formed, then it was too short-lived to be resolved in that system (<ms). They also observed one intermediate in the CuAAC reaction with a relatively long lifetime (~4.5 s), which was formed irreversibly, and tentatively assigned as a copper triazolide (**15** in Figure 4A). In contrast to this previous study, the methionine-modified α-HL nanopores developed in the present work yielded data with a higher signal-to-noise ratio, which enabled key transient intermediates in the CuAAC reaction to be resolved (*vide infra*).

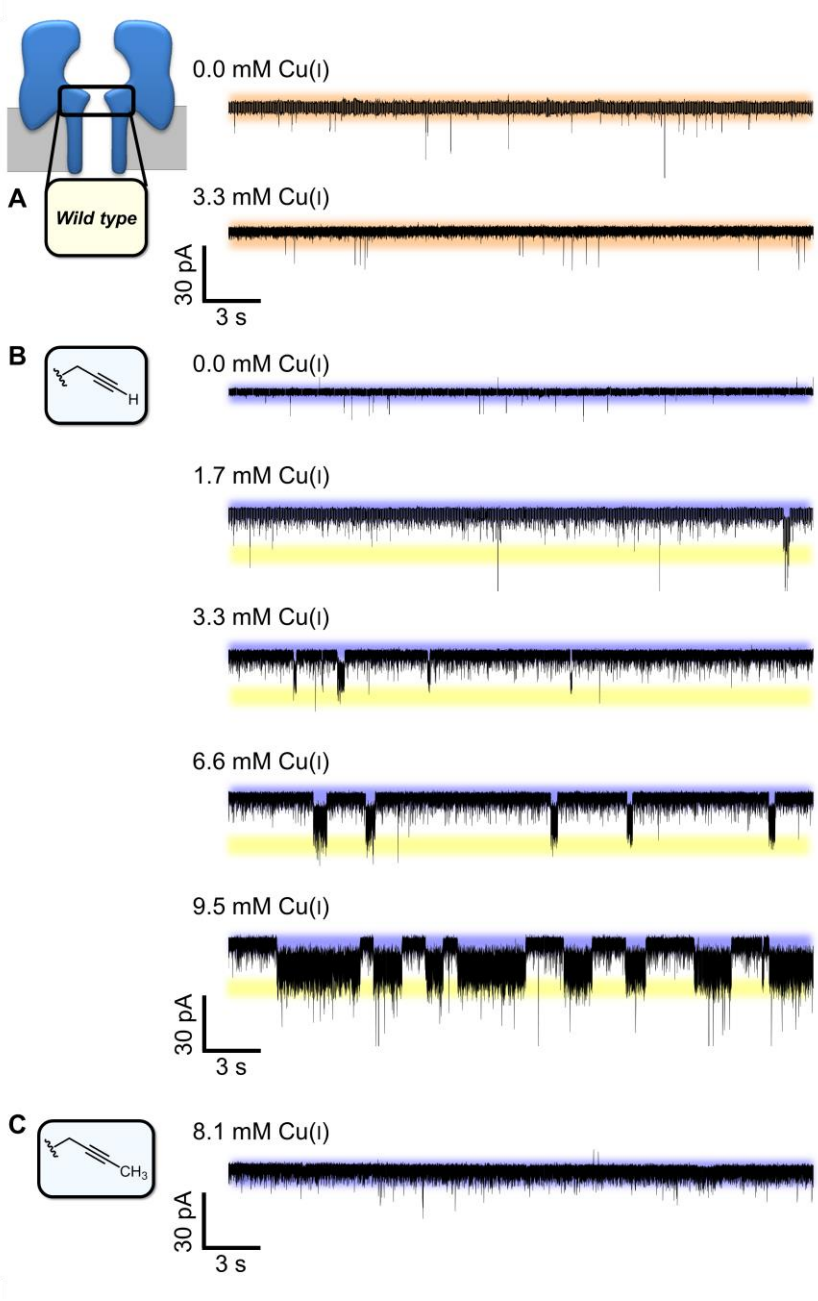

Figure 5. Influence of Cu(I) on ion currents in wild-type and alkyne-modified nanopores. (A) No change was seen upon addition of Cu(I) to a wild-type α-HL nanopore. (B) In a nanopore modified with a terminal alkyne, introduction of Cu(I) caused increased noise (black) due to short-lived events which are not fully resolved, as well as longer-duration, well-resolved step-wise blockages (yellow). The frequency and duration of the resolved events was dependent on

the concentration of Cu(I). (C) A nanopore modified with an internal alkyne also displayed increased noise in the presence of Cu(I), but the longer-duration (yellow) events were absent. All traces were recorded at 298 K, +100 mV in 1 M KCl, 30 mM potassium phosphate buffer (pH 8.0). Data were filtered using a 2 kHz hardware Bezel filter, no additional software filter was applied.

Initially, we sought to examine the reversible blockages observed in alkyne-modified nanopores (Figure 3B, yellow) by varying the concentration of Cu(I) (Figure 5 and S41–S44). Due to the ion current being dominated by the background of 1 M KCl electrolyte solution in which the experiments were performed, the addition of up to 10 mM of Cu(I) had a minimal effect on the magnitude of the recorded ion currents. However, increasing the concentration of Cu(I) in the presence of an alkyne-functionalized nanopore led to an increase in noise, while the frequency and duration of the reversible, stepped current blockages previously identified in Figure 3B also increased (yellow, Figure 5B). The copper-dependent increase in noise (shallow events with <ms durations) was not observed in wild-type α-HL nanopores (Figure 5B *cf.* 5A). In contrast, a nanopore functionalized with the methyl-terminated internal alkyne **4** also displayed increased noise in the presence of Cu(I), but none of the longer-duration events (no yellow state in Figure 5C and S45). Since this internal alkyne is unable to form a terminal σ-type copper acetylide (resembling **13**), then the noise observed in the traces shown in Figure 5B can be attributed to the reversible formation of the cationic copper π-complex of both the terminal and internal alkynes (**12′** and **11′** in Figures 4A and 4B, respectively).

Having assigned the blue levels in Figure 5B as incorporating **12** and its copper π-complex

12′, we then turned to assigning the reversible current blockages (yellow in Figure 5B). The increase in the population of these stepped current blockages on increasing the Cu(I) concentration is also consistent with the involvement of copper. The increased duration of these events with increasing Cu(I) concentration means that such events cannot be attributed to the simple bimolecular dissociation of **13′** → **13** + Cu^+, since the lifetime of the bis-Cu complex **13′** should be independent of the Cu(I) concentration. Instead, such a copper-dependent increase in event duration would be consistent with the noisy yellow events being attributed to both alkyne species in the **13** ⇌ **13′** equilibrium, since increasing the copper concentration shifts this equilibrium to the right and therefore slow down the reverse reaction **13** → **12′** (yellow to blue in Figure 5B).

We reasoned that a more detailed analysis might enable resolution of the two species contributing to each of the noisy **12** ⇌ **12′** (blue) and **13** ⇌ **13′** (yellow) states. Pleasingly, all-points histogram analysis (see SI section 2.8.1) of the complete ion current traces exemplified in Figure 5 revealed that both the yellow and blue states each consisted of two Gaussian distributions of sub-states (Figure 6, S52 and Tables S2–S5). In addition, the proportions of both sub-populations were found to shift as the concentration of Cu(I) was varied. At [Cu(I)] = 6.6 mM, the blue sub-populations assigned to **12** ⇌ **12′** had equal integrals, indicating that the corresponding equilibrium constant $K_1 \approx 150\ M^{-1}$ at +100 mV (Figure 6C). Similarly, at [Cu(I)] = 3.3 mM, the yellow sub-populations assigned to **13** ⇌ **13′** had equal integrals, indicating that the associated equilibrium constant $K_3 \approx 300\ M^{-1}$ at +100 mV. Indeed, complete modelling of these sequential equilibria at +100 mV yielded values of $K_1 = 162\ M^{-1}$, $K_2 = 0.22$, $K_3 = 303\ M^{-1}$ by

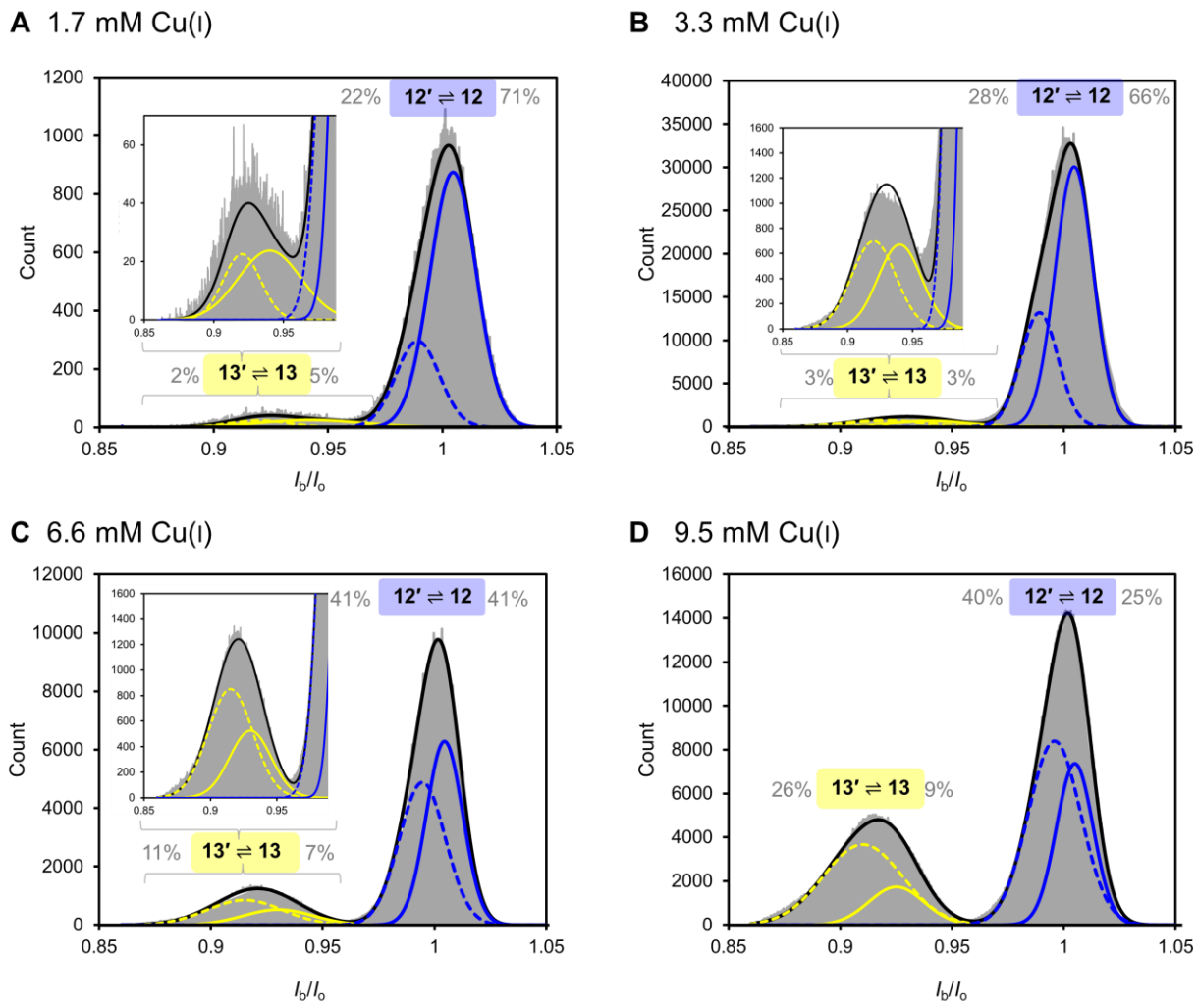

Figure 6. (A–D) All-points histogram analysis of the blue and yellow ion current levels resolved two Cu(I)-dependent Gaussian distributions of states corresponding to alkyne species **12**, **12′**, **13** and **13′** at varying copper concentrations. (E) The populations of **12**, **12′**, **13** and **13′** states as the concentration of Cu(I) was varied (circles) was used to determine the equilibrium constants K_1, K_2, and K_3 and the corresponding modelled speciation diagram (lines). Fitting details are provided in Section 2.8 in the SI; both graphical and iterative fitting of the populations yielded similar fits (Table S6 and Figure S56). Data obtained at +100 mV in 1 M KCl, 30 mM potassium phosphate buffer (pH 8.0).

graphical fitting, and K_1 = 168 M^{-1}, K_2 = 0.12, K_3 = 292 M^{-1} by iterative fitting approaches (section 2.8 SI). Moreover, it was also possible to construct the associated speciation plots revealing the expected population of states as the concentration as Cu(I) was varied (Figures 6E and S56). The difference between the copper π-complexation equilibrium constants K_1 and K_3 is consistent with the increased electron density of the π-system in the Cu-terminal alkyne **13** compared to the H-terminal alkyne **12**, and with the increased covalency of the bis-copper complex **13′** compared to the H-terminal alkyne complex **12′** (Figure S56). Furthermore, our observation of copper π-complexation in **12** ⇌ **12′** and **13** ⇌ **13′** being rapid (and hence noisy) compared to the kinetically well-resolved rearrangement in **12′** ⇌ **13** is consistent with previous mechanistic investigations.[43,46,47]

It is important to note that nanopore analyses are unusual in that experiments are performed under an applied electric potential, meaning that the rate and selectivity of reactions may be influenced by the external electric field.[53-58] Indeed, the populations presented in Figure 6 were determined at a potential of +100 mV, and therefore likely to differ from the non-field perturbed conditions under which chemical reactions are normally performed. Thus, we next set out to examine how lowering the applied voltage would influence the population of states. Lowering the potential lowers the ion current flowing through the pore and therefore the signal-to-noise ratio, making analysis of the type presented in Figure 6 more challenging. Thus, we instead performed a simpler analysis of the voltage-dependency of exchange between the well-resolved **12** ⇌ **12′** (blue) and **13** ⇌ **13′** (yellow) states at a constant concentration of Cu(I) (Figure 7 and S46–S50). The observed voltage-dependencies of the relative populations (K_{obs}) and rates of

exchange between the blue and yellow states ($1/\tau_{on}$ and $1/\tau_{off}$) were found to be consistent with the respective assignments to the **12** ⇌ **12′** and **13** ⇌ **13′** equilibria. The application of a positive voltage shifts both the **12** ⇌ **12′** and **13** ⇌ **13′** equilibria to left due to destabilization of the cationic copper π-complexes. Thus, increasing the voltage decreases proportion of time spent in the **12′** state, thereby decreasing the rate of the forward reaction of **12′** → **13** ($1/\tau_{on}$, blue to yellow in Figure 7). Conversely, the increased proportion of time spent in the **13** state at higher voltages increases the rate of the backwards reaction of **13** → **12′** ($1/\tau_{off}$, yellow to blue in Figure 7). As a result of these changes in the rates of the forward and reverse reactions, there is a corresponding decrease in the apparent equilibrium ratio K_{obs} between the **12** ⇌ **12′** (blue) and **13** ⇌ **13′** states (yellow) as the voltage is increased. For instance, the preference for the **13** ⇌ **13′** level is decreased by ~three orders of magnitude at +100 mV compared to non-field perturbed conditions ($V = 0$, Figure 7C).

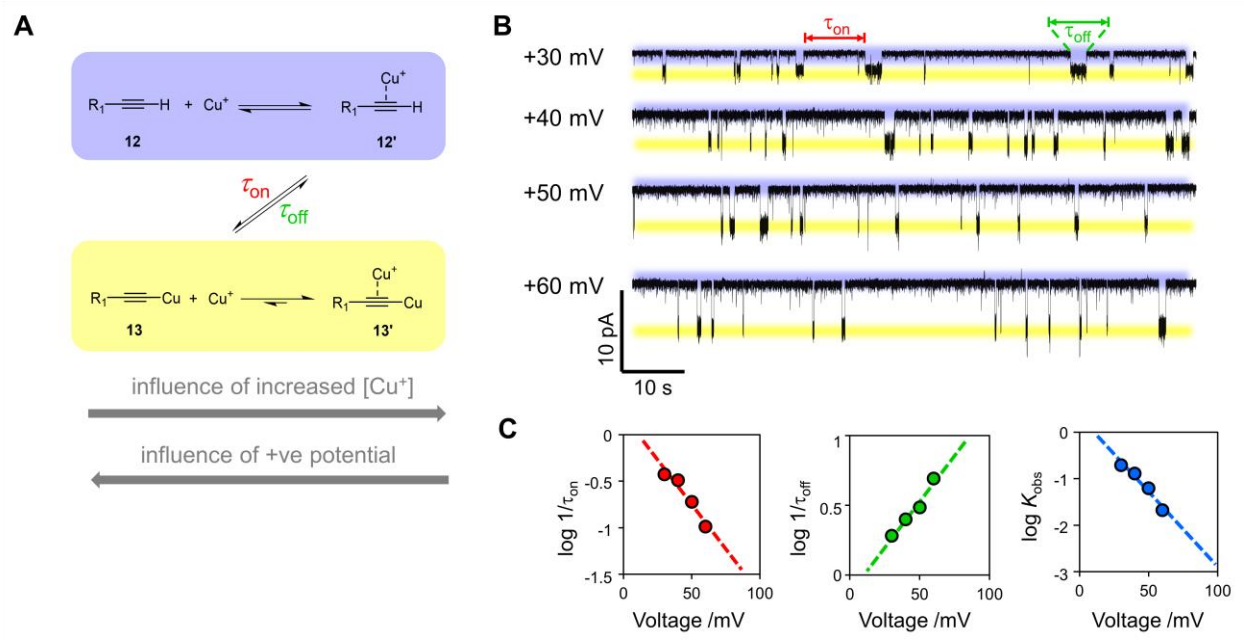

Figure 7. (A) Experimental evaluation of the effect of the applied electric field on exchange between the **12** ⇌ **12′** (blue) and **13** ⇌ **13′** (yellow) copper-dependent intermediates in alkyne-modified nanopores. (B) Sample ion current traces are shown at different voltages (more data are provided in the SI). (C) The voltage dependence of τ_{on}^{-1}, τ_{off}^{-1}, and K_{obs} is shown in the colored graph insets. Conditions: $CuSO_4$ (0.82 mM), sodium ascorbate (8.2 mM), 1 M KCl, 30 mM potassium phosphate buffer (pH 8.0) at 298 K. Histogram data and data fitting are provided in Figure S50.

It follows that the population of the cationic **13'** sub-population should also be favored compared to conditions in which a (destabilizing) positive potential is applied. Indeed, the application of negative potentials to an alkyne-modified pore in the presence of Cu(I) gave rise to long-lived blockage events with durations of several seconds (Figure S51). It should be noted that the rates and equilibrium constants under these conditions are not directly comparable to the experiments presented in Figure 7 (due to the requirement to add reagents to the opposite side of the nanopore under negative potentials). Nonetheless, only a single, low-noise state was

observed at –60 mV, which was consistent with electrostatic trapping of **13′** (Figure S51C). The decrease in noise on increasing the magnitude of the applied negative potential was also commensurate with minimal fluctuation between the stabilized cationic copper π-complex **13′** and copper acetylide **13**.

Having fully assigned the identity of the reversible intermediates in the sequential equilibria **12** ⇌ **12′** ⇌ **13** ⇌ **13′**, our attention turned to assigning the intermediate (green) level, which was always seen to proceed the irreversible formation of the (red) triazole product (Figures 3B and 8). Indeed, such an ordering of events was seen across all substrates examined (Figure 3B and Supporting Information). It is known from detailed mechanistic investigations that the proposed reactive intermediates between the bis-Cu acetylide (**13′**, yellow) and the Cu-triazolide (**15**, green) are extremely short lived, even in the presence of stabilizing ligands,[43,46] and it seems reasonable that the state (green in Figures 3B and 8) immediately preceding the final triazole product (red in Figures 3B and 8) can be attributed to Cu-triazolide **15**. Such an

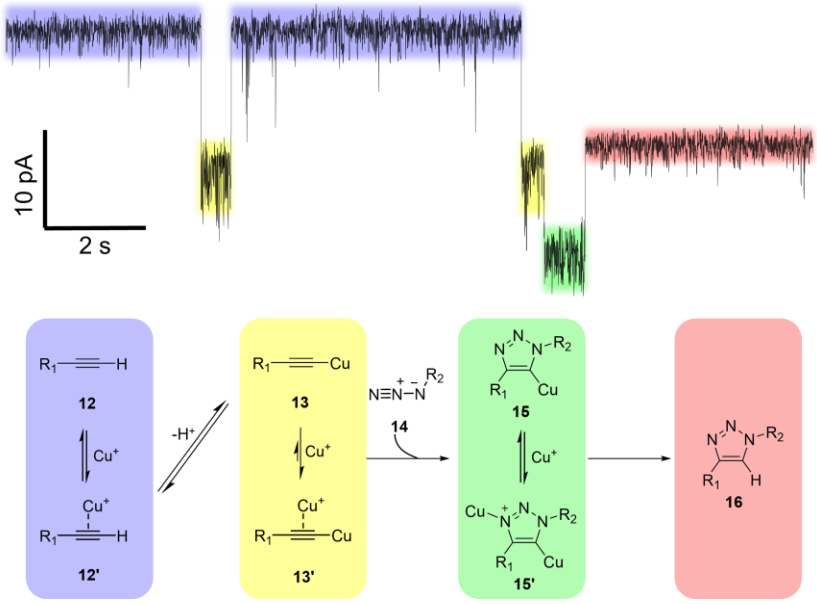

Figure 8. Expanded view of ion current changes during a CuAAC reaction taking place between an alkyne-bearing nanopore and azide **7**. Data obtained at +100 mV in 1 M KCl, 30 mM potassium phosphate buffer (pH 8.0) at 298 K. See the SI for the full trace, other examples and detailed experimental conditions.

assignment is in agreement with the previous assignment of the intermediate previously observed in CuAAC reactions at the single-molecule level.[18] It also seems reasonable to attribute the noisy character of this green intermediate to **15** ⇌ **15′** copper π-complexation, even though its short-lived and irreversible nature precludes analysis of the type presented in Figure 6. Indeed, like the copper-acetylide **13**, Cu-triazolide **15** also possesses increased electron density (and basicity) compared to its non-cuprated equivalent, the final triazole product **16**.

Our single-molecule analysis of the rapidly equilibrating copper-associated intermediates in the CuAAC mechanism are consistent the hypothesis emerging from ensemble investigations that most CuAAC reactions proceed *via* a bis-Cu mechanism.[43,46,52] While previous

investigations of transient intermediates in the CuAAC reaction have required the use of stabilizing ligands, this study demonstrates the ability of synthetically functionalized nanopores to observe short-lived and dynamically exchanging reaction intermediates under typical reaction conditions.

CONCLUSION

We have demonstrated the use of methionine-modification as a site-selective method to enable the synthetic diversification of α-HL protein nanopores. The installation of reactive linkers within the channel enabled nanopores to be synthetically diversified *via* bio-orthogonal click reactions with a range of small molecules, nucleotides and nucleic acids. Notably, this method of nanopore modification complements alternative approaches that use site-directed mutagenesis or native chemical ligation to install new functionalities within nanopores, while also offering superior site selectivity compared to other *in situ* synthetic pore modification protocols.[34] In particular, the ability to use both the azide and alkyne oxaziridine linkers expands the potential for orthogonal functionalization using existing libraries of commercially available alkyne and azide coupling partners.

An unexpected outcome of the *in situ* structural diversification was the ability to resolve the trajectory of reactions at the single-molecule level, by observing transient intermediates that are hard to detect using ensemble techniques. Moreover, it was even possible to resolve species involved in rapidly exchanging (sub-millisecond) equilibria, and to determine individual equilibrium constants and the associated changes in speciation as the reaction conditions were

varied. Indeed, the modification chemistry introduced here is highly versatile, rapid and accessible, and may provide a useful platform for implementing physical organic mechanistic investigation at the single-molecule level.

EXPERIMENTAL SECTION

Single Channel Experiment Setup

Single channel experiments were performed in a custom-built cell (Figure S2 and associated text). A hanging drop of hexadecane in *n*-pentane (5 μL, 10%, *v*/*v*) was touched on each side of the Teflon sheet containing an aperture and allowed to dry for 1 minute. KCl/potassium phosphate buffer (600 μL) was added to the well each side of the aperture. Lipid (1,2-diphytanoyl-*sn*-glycero-3-phosphocholine) (approx. 8 μL, 10 μg μL^{-1} in *n*-pentane) was added to each side of the well, and left for approx. 5 mins to allow the pentane to evaporate. The cell was subsequently placed into a Faraday cage and Ag/AgCl electrodes (Warner), connected to a patch clamp amplifier (Axopatch 200B, Molecular Devices), were suspended either side of the Teflon sheet. The buffer solution on both sides of the Teflon sheet was aspirated and dispensed using a Hamilton syringe to 'paint' a phospholipid bilayer across the aperture. A ±1 mV pulse was applied at 1333 Hz to determine when a bilayer was obtained (capacitance >30 pF). The membrane was characterized with successive 2 second sweeps under an applied potential ranging from +100 to −100 mV. The membrane was deemed acceptable if the range of current flow across the membrane measured <1 pA. A gel loading tip fitted to a 20 μL pipette was introduced

into an aqueous solution of α-HL (approx. 250 μM (5 μL of the storage solution diluted with 45 μL of water)), without aspirating, such that a tiny amount (<1 μL) of the solution remained on the tip. Under an applied voltage of +100 mV, the α-HL was then fired at the aperture. If after at least 1 minute no channel insertion was observed, then this process was repeated until a single channel arose. The single nanopore was characterized by at least four 2-second I/V sweeps (−100 to +100 mV, Figure S4), showing the characteristic asymmetry at positive *vs* negative voltages.

Methionine Modification of Protein Nanopore

A fresh solution of oxaziridine reagent **1**–**4** was made by dissolving the reagent in DMSO to a concentration of 100 mM. Under an applied voltage (+100 mV), oxaziridine reagent solution (1 μL) was added to either the *cis* or *trans* well of a single-channel experiment (see Figure S3; final well concentration of reagent ~0.17 mM). The contents of the well were briefly mixed by aspirating and plunging with a 50 μL pipette three times. Upon observing a ~3% drop in the pore ion current, indicating a single methionine modification, a solution of methionine (250 mM, 8 μL, 20 equiv.) was immediately added to the same well, aiming the micropipette tip towards the location of the aperture. The contents of the well were mixed by repeated micropipette aspiration and plunging (5 × 50 μL). If no further quantized drops in the ion current (indicating further methionine modifications) were observed after 5 min, the singly modified pore was characterized by at least four I/V sweeps (−100 to +100 mV).

CuAAC Reaction of Alkyne-modified Protein Nanopore

Under an applied voltage (+100 mV), a solution of $CuSO_4$ (1 μL, 1 M, final concentration ~1.7 mM) was added to the *trans* well of a single-channel experiment with an alkyne-modified protein nanopore. A freshly made solution of sodium ascorbate (2 μL, 1 M, final concentration ~3.4 mM) was added, and the contents of the well were mixed by micropipette aspirating and plunging (10 × 50 μL). Complete reduction to Cu(I) was evident by disappearance of the blue colour of the buffer. When reversible formation of a copper acetylide became apparent in the current trace, a solution of azide (1–2 μL, 1 M) was added to the *trans* well (if carrying a positive charge at pH 8) or the *cis* well (if carrying a negative charge at pH 8). The contents of the well was carefully mixed by micropipette aspirating and plunging (1–2 × 50 μL), or the azide was left to diffuse across the well. The experiment was left until a permanent drop in the pore current and cessation of reversible events indicated a CuAAC reaction had taken place. The modified pore was characterized by at least four I/V sweeps (−100 to +100 mV).

CuAAC Reaction of Azide-modified Protein Nanopore

Under an applied voltage (+100 mV), a solution of $CuSO_4$ (1 μL, 1 M, final concentration ~1.7 mM) was added to the *trans* well (if using an alkyne reagent carrying a positive charge at pH 8) or the *cis* well (if using an alkyne carrying a negative charge at pH 8) of a single-channel experiment with an azide-modified protein nanopore. A freshly made solution of sodium ascorbate (2 μL, 1 M, final concentration ~3.4 mM) was added to the same well, and the contents of the well were mixed by micropipette aspirating and plunging (10 × 50 μL). Complete

reduction to Cu(I) was evident by disappearance of the blue colour of the buffer. A solution of alkyne reagent (2 μL, 1 M) was added to the same well, and the contents of the well was carefully mixed by micropipette aspirating and plunging (1–2 × 50 μL). The experiment was left until a permanent drop in the pore current indicated a CuAAC reaction had taken place. The modified pore was characterized by at least four I/V sweeps (−100 to +100 mV).

SPAAC Reaction of Azide-modified Nanopore

Under an applied voltage (+100 mV), a solution of cyclooctyne **10** (10 μL, 100 mM, final concentration ~1.7 mM) was added to both wells of a single-channel experiment with an azide-modified protein nanopore. The contents of the well were mixed by micropipette aspirating and plunging (5 × 50 μL). The experiment was left until a permanent drop in the pore current indicated a SPAAC reaction had taken place. The modified pore was characterized by at least four I/V sweeps (−100 to +100 mV).

ASSOCIATED CONTENT

Supporting Information. The Supporting Information is available free of charge on the ACS Publications website at DOI: 10.1021/acsnano.XXXX. Experimental setup; synthetic procedures; full nanopore current traces; experimental details; detailed data analysis; Figures S1−S74; Tables S1−S6.

AUTHOR INFORMATION

Corresponding Author

* scott.cockroft@ed.ac.uk

Author Contributions

The manuscript was written through contributions of all authors. All authors have given approval to the final version of the manuscript.

ACKNOWLEDGMENT

We thank the ERC Starting Grant 336935 “Transmembrane molecular machines” for funding.

REFERENCES

(1) Bayley, H.; Cremer, P. S., Stochastic Sensors Inspired by Biology. *Nature* **2001**, *413*, 226-230.
(2) Schmidt, J., Stochastic Sensors. *J. Mater. Chem.* **2005**, *15*, 831-840.
(3) Lin, Y.; Ying, Y. L.; Gao, R.; Long, Y. T., Single-Molecule Sensing with Nanopore Confinement: From Chemical Reactions to Biological Interactions. *Chem. Eur. J.* **2018**, *24*, 13064-13071.
(4) Cao, C.; Long, Y. T., Biological Nanopores: Confined Spaces for Electrochemical Single-Molecule Analysis. *Acc Chem Res* **2018**, *51*, 331-341.
(5) Dekker, C., Solid-State Nanopores. *Nat. Nanotechnol.* **2007**, *2*, 209-215.
(6) Tagliazucchi, M. In *Chemically Modified Nanopores and Nanochannels*; Tagliazucchi, M., Szleifer, I., Eds.; William Andrew Publishing: Boston, 2017, p 1-25.
(7) Howorka, S., Building Membrane Nanopores. *Nat. Nanotechnol.* **2017**, *12*, 619-630.
(8) Cooper, J. A.; Borsley, S.; Lusby, P. J.; Cockroft, S. L., Discrimination of Supramolecular Chirality Using a Protein Nanopore. *Chem. Sci.* **2017**, *8*, 5005-5009.
(9) Ramsay, W. J.; Bayley, H., Single-Molecule Determination of the Isomers of D-Glucose and D-Fructose That Bind to Boronic Acids. *Angew. Chem., Int. Ed.* **2018**, *57*, 2841-2845.
(10) Johnson, R. P.; Fleming, A. M.; Perera, R. T.; Burrows, C. J.; White, H. S., Dynamics of a DNA Mismatch Site Held in Confinement Discriminate Epigenetic Modifications of Cytosine. *J. Am. Chem. Soc.* **2017**, *139*, 2750-2756.
(11) Johnson, R. P.; Fleming, A. M.; Beuth, L. R.; Burrows, C. J.; White, H. S., Base Flipping within the Alpha-Hemolysin Latch Allows Single-Molecule Identification of Mismatches in DNA. *J. Am. Chem. Soc.* **2016**, *138*, 594-603.
(12) Borsley, S.; Cooper, J. A.; Lusby, P. J.; Cockroft, S. L., Nanopore Detection of Single-Molecule Binding within a Metallosupramolecular Cage. *Chem. Eur. J.* **2018**, *24*, 4542-4546.

(13) Ying, Y. L.; Zhang, J.; Meng, F. N.; Cao, C.; Yao, X.; Willner, I.; Tian, H.; Long, Y. T., A Stimuli-Responsive Nanopore Based on a Photoresponsive Host-Guest System. *Sci. Rep.* **2013**, *3*, 1662.
(14) Chu, J.; Gonzalez-Lopez, M.; Cockroft, S. L.; Amorin, M.; Ghadiri, M. R., Real-Time Monitoring of DNA Polymerase Function and Stepwise Single-Nucleotide DNA Strand Translocation through a Protein Nanopore. *Angew. Chem., Int. Ed.* **2010**, *49*, 10106-10109.
(15) Meng, F. N.; Li, Z. Y.; Ying, Y. L.; Liu, S. C.; Zhang, J.; Long, Y. T., Structural Stability of the Photo-Responsive DNA Duplexes Containing One Azobenzene *via* a Confined Pore. *Chem. Commun.* **2017**, *53*, 9462-9465.
(16) Wu, H. C.; Bayley, H., Single-Molecule Detection of Nitrogen Mustards by Covalent Reaction within a Protein Nanopore. *J. Am. Chem. Soc.* **2008**, *130*, 6813-6819.
(17) Steffensen, M. B.; Rotem, D.; Bayley, H., Single-Molecule Analysis of Chirality in a Multicomponent Reaction Network. *Nat. Chem.* **2014**, *6*, 603-607.
(18) Lee, J.; Bayley, H., Semisynthetic Protein Nanoreactor for Single-Molecule Chemistry. *Proc. Natl. Acad. Sci. U. S. A.* **2015**, *112*, 13768-13773.
(19) Lee, J.; Boersma, A. J.; Boudreau, M. A.; Cheley, S.; Daltrop, O.; Li, J.; Tamagaki, H.; Bayley, H., Semisynthetic Nanoreactor for Reversible Single-Molecule Covalent Chemistry. *ACS Nano* **2016**, *10*, 8843-8850.
(20) Qing, Y.; Pulcu, G. S.; Bell, N. A. W.; Bayley, H., Bioorthogonal Cycloadditions with Sub-Millisecond Intermediates. *Angew. Chem., Int. Ed.* **2018**, *57*, 1218-1221.
(21) Shin, S. H.; Steffensen, M. B.; Claridge, T. D.; Bayley, H., Formation of a Chiral Center and Pyrimidal Inversion at the Single-Molecule Level. *Angew. Chem., Int. Ed.* **2007**, *46*, 7412-7416.
(22) Ren, H.; Cheyne, C. G.; Fleming, A. M.; Burrows, C. J.; White, H. S., Single-Molecule Titration in a Protein Nanoreactor Reveals the Protonation/Deprotonation Mechanism of a C:C Mismatch in DNA. *J. Am. Chem. Soc.* **2018**, *140*, 5153-5160.
(23) Tan, C. S.; Riedl, J.; Fleming, A. M.; Burrows, C. J.; White, H. S., Kinetics of T3-DNA Ligase-Catalyzed Phosphodiester Bond Formation Measured Using the Alpha-Hemolysin Nanopore. *ACS Nano* **2016**, *10*, 11127-11135.
(24) Watson, M. A.; Cockroft, S. L., An Autonomously Reciprocating Transmembrane Nanoactuator. *Angew. Chem., Int. Ed.* **2016**, *55*, 1345-1349.
(25) Watson, M. A.; Cockroft, S. L., Man-Made Molecular Machines: Membrane Bound. *Chem. Soc. Rev.* **2016**, *45*, 6118-6129.
(26) Qing, Y.; Ionescu, S. A.; Pulcu, G. S.; Bayley, H., Directional Control of a Processive Molecular Hopper. *Science* **2018**, *361*, 908-912.
(27) Miles, B. N.; Ivanov, A. P.; Wilson, K. A.; Dogan, F.; Japrung, D.; Edel, J. B., Single Molecule Sensing with Solid-State Nanopores: Novel Materials, Methods, and Applications. *Chem. Soc. Rev.* **2013**, *42*, 15-28.
(28) Anderson, B. N.; Muthukumar, M.; Meller, A., pH Tuning of DNA Translocation Time through Organically Functionalized Nanopores. *ACS Nano* **2013**, *7*, 1408-1414.

(29) Wanunu, M.; Meller, A., Chemically Modified Solid-State Nanopores. *Nano Lett.* **2007**, *7*, 1580-1585.
(30) Ali, M.; Ramirez, P.; Nguyen, H. Q.; Nasir, S.; Cervera, J.; Mafe, S.; Ensinger, W., Single Cigar-Shaped Nanopores Functionalized with Amphoteric Amino Acid Chains: Experimental and Theoretical Characterization. *ACS Nano* **2012**, *6*, 3631-3640.
(31) Wu, H. C.; Astier, Y.; Maglia, G.; Mikhailova, E.; Bayley, H., Protein Nanopores with Covalently Attached Molecular Adapters. *J. Am. Chem. Soc.* **2007**, *129*, 16142-16148.
(32) Rincon-Restrepo, M.; Mikhailova, E.; Bayley, H.; Maglia, G., Controlled Translocation of Individual DNA Molecules through Protein Nanopores with Engineered Molecular Brakes. *Nano Lett.* **2011**, *11*, 746-750.
(33) Song, L.; Hobaugh, M. R.; Shustak, C.; Cheley, S.; Bayley, H.; Gouaux, J. E., Structure of Staphylococcal A-Hemolysin, a Heptameric Transmembrane Pore. *Science* **1996**, *274*, 1859-1865.
(34) Borsley, S.; Cockroft, S. L., *In Situ* Synthetic Functionalization of a Transmembrane Protein Nanopore. *ACS Nano* **2018**, *12*, 786-794.
(35) Lin, S.; Yang, X.; Jia, S.; Weeks, A. M.; Hornsby, M.; Lee, P. S.; Nichiporuk, R. V.; Iavarone, A. T.; Wells, J. A.; Toste, F. D.; Chang, C. J., Redox-Based Reagents for Chemoselective Methionine Bioconjugation. *Science* **2017**, *355*, 597-602.
(36) Buchsbaum, S. F.; Mitchell, N.; Martin, H.; Wiggin, M.; Marziali, A.; Coveney, P. V.; Siwy, Z.; Howorka, S., Disentangling Steric and Electrostatic Factors in Nanoscale Transport through Confined Space. *Nano Lett.* **2013**, *13*, 3890-3896.
(37) Zheng, T.; Rouhanifard, S. H.; Jalloh, A. S.; Wu, P., Click Triazoles for Bioconjugation. *Top. Heterocycl. Chem.* **2012**, *28*, 163-183.
(38) Pickens, C. J.; Johnson, S. N.; Pressnall, M. M.; Leon, M. A.; Berkland, C. J., Practical Considerations, Challenges, and Limitations of Bioconjugation *via* Azide-Alkyne Cycloaddition. *Bioconjugate Chem.* **2018**, *29*, 686-701.
(39) Li, L.; Zhang, Z., Development and Applications of the Copper-Catalyzed Azide-Alkyne Cycloaddition (CuAAC) as a Bioorthogonal Reaction. *Molecules* **2016**, *21*, 1393.
(40) Stoddart, D.; Maglia, G.; Mikhailova, E.; Heron, A. J.; Bayley, H., Multiple Base-Recognition Sites in a Biological Nanopore: Two Heads Are Better Than One. *Angew. Chem., Int. Ed.* **2010**, *49*, 556-559.
(41) Deamer, D.; Akeson, M.; Branton, D., Three Decades of Nanopore Sequencing. *Nat. Biotechnol.* **2016**, *34*, 518-524.
(42) Bayley, H., Nanopore Sequencing: From Imagination to Reality. *Clin. Chem.* **2015**, *61*, 25-31.
(43) Jin, L.; Tolentino, D. R.; Melaimi, M.; Bertrand, G., Isolation of Bis(Copper) Key Intermediates in Cu-Catalyzed Azide-Alkyne "Click Reaction". *Sci. Adv.* **2015**, *1*, e1500304.
(44) Ben El Ayouchia, H.; Bahsis, L.; Anane, H.; Domingo, L. R.; Stiriba, S.-E., Understanding the Mechanism and Regioselectivity of the Copper(I) Catalyzed [3 + 2] Cycloaddition Reaction between Azide and Alkyne: A Systematic DFT Study. *RSC Adv.* **2018**, *8*, 7670-7678.

(45) Zhu, L.; Brassard, C. J.; Zhang, X.; Guha, P. M.; Clark, R. J., On the Mechanism of Copper(I)-Catalyzed Azide-Alkyne Cycloaddition. *Chem. Rec.* **2016**, *16*, 1501-1517.
(46) Worrell, B. T.; Malik, J. A.; Fokin, V. V., Direct Evidence of a Dinuclear Copper Intermediate in Cu(I)-Catalyzed Azide-Alkyne Cycloadditions. *Science* **2013**, *340*, 457-460.
(47) Rodionov, V. O.; Fokin, V. V.; Finn, M. G., Mechanism of the Ligand-Free Cui-Catalyzed Azide-Alkyne Cycloaddition Reaction. *Angew. Chem., Int. Ed.* **2005**, *44*, 2210-2215.
(48) Ahlquist, M.; Fokin, V. V., Enhanced Reactivity of Dinuclear Copper(I) Acetylides in Dipolar Cycloadditions. *Organometallics* **2007**, *26*, 4389-4391.
(49) Kuang, G. C.; Guha, P. M.; Brotherton, W. S.; Simmons, J. T.; Stankee, L. A.; Nguyen, B. T.; Clark, R. J.; Zhu, L., Experimental Investigation on the Mechanism of Chelation-Assisted, Copper(Ii) Acetate-Accelerated Azide-Alkyne Cycloaddition. *J. Am. Chem. Soc.* **2011**, *133*, 13984-14001.
(50) Himo, F.; Lovell, T.; Hilgraf, R.; Rostovtsev, V. V.; Noodleman, L.; Sharpless, K. B.; Fokin, V. V., Copper(I)-Catalyzed Synthesis of Azoles. DFT Study Predicts Unprecedented Reactivity and Intermediates. *J. Am. Chem. Soc.* **2005**, *127*, 210-216.
(51) Berg, R.; Straub, B. F., Advancements in the Mechanistic Understanding of the Copper-Catalyzed Azide-Alkyne Cycloaddition. *Beilstein J. Org. Chem.* **2013**, *9*, 2715-2750.
(52) Iacobucci, C.; Reale, S.; Gal, J. F.; de Angelis, F., Dinuclear Copper Intermediates in Copper(I)-Catalyzed Azide-Alkyne Cycloaddition Directly Observed by Electrospray Ionization Mass Spectrometry. *Angew. Chem., Int. Ed.* **2015**, *54*, 3065-3068.
(53) Shaik, S.; Ramanan, R.; Danovich, D.; Mandal, D., Structure and Reactivity/Selectivity Control by Oriented-External Electric Fields. *Chem. Soc. Rev.* **2018**, *47*, 5125-5145.
(54) Shaik, S.; Mandal, D.; Ramanan, R., Oriented Electric Fields as Future Smart Reagents in Chemistry. *Nat. Chem.* **2016**, *8*, 1091-1098.
(55) Welborn, V. V.; Ruiz Pestana, L.; Head-Gordon, T., Computational Optimization of Electric Fields for Better Catalysis Design. *Nat. Catalysis* **2018**, *1*, 649-655.
(56) Wang, Z.; Danovich, D.; Ramanan, R.; Shaik, S., Oriented-External Electric Fields Create Absolute Enantioselectivity in Diels-Alder Reactions: Importance of the Molecular Dipole Moment. *J. Am. Chem. Soc.* **2018**, *140*, 13350-13359.
(57) Ramanan, R.; Danovich, D.; Mandal, D.; Shaik, S., Catalysis of Methyl Transfer Reactions by Oriented External Electric Fields: Are Gold-Thiolate Linkers Innocent? *J. Am. Chem. Soc.* **2018**, *140*, 4354-4362.
(58) Ciampi, S.; Darwish, N.; Aitken, H. M.; Diez-Perez, I.; Coote, M. L., Harnessing Electrostatic Catalysis in Single Molecule, Electrochemical and Chemical Systems: A Rapidly Growing Experimental Tool Box. *Chem. Soc. Rev.* **2018**, *47*, 5146-5164.

GRAPHICAL TOC ENTRY: